International Journal of Microwave and Wireless Technologies, 2016, 8(8), 1253–1263.
doi:10.1017/S1759078715000847

RESEARCH PAPER

Circularly polarized microstrip antenna arrays with reduced mutual coupling using metamaterial

R. HAFEZIFARD[1], JALIL RASHED-MOHASSEL[2], MOHAMMAD NASER-MOGHADASI[1] AND R. A. SADEGHZADEH[3]

A circularly polarized (CP) and high gain Microstrip antenna is designed in this paper using metamaterial concepts. The antenna, built on a metamaterial substrate, showed significant size reduction and less mutual coupling in an array compared with similar arrays on conventional substrates. Demonstrated to have left-handed magnetic characteristics, the methodology uses complementary split-ring resonators (SRRs) placed horizontally between the patch and the ground plane. In order to reduce mutual coupling in the array structure, hexagonal-SRRs are embedded between antenna elements. The procedure is shown to have great impact on the antenna performance specifically its bandwidth which is broadened from 400 MHz to 1.2 GHz for X-band and as well as its efficiency. The structure has also low loss and improved standing wave ratio and less mutual coupling. The results show that a reduction of 26.6 dB in mutual coupling is obtained between elements at the operation frequency of the array. Experimental data show a reasonably good agreement between simulation and measured results.

Keywords: Circularly polarized, Microstrip antenna, Metamaterial structures, Mutual coupling, Split-ring resonators, Hexagonal-SRRs

Received 19 October 2014; Revised 13 April 2015; Accepted 17 April 2015; first published online 30 June 2015

I. INTRODUCTION

Circularly polarized (CP) array antennas have been the subject of interest for many years, due to the requirement for greater penetration and coverage in wireless and satellite communications. Early implementations of omnidirectional CP were made by stepped impedance stub (SIS), loaded stepped impedance resonators (SIR), SIS loaded hexagon SIR [1] or by using a proper asymmetry within the annular-ring slot structure and feeding the annular-ring slot using a slot line feed [2]. Also, these antennas are useful in numerous applications such as surveillance, interference mitigation, Synthetic Aperture Radar (SAR) sensor, radars and Global Navigation Satellite System (GNSS) remote sensing particularly at S- and X-bands [3–9].

On the other hand, mutual coupling between array elements affects both the embedded element radiation pattern and the element input impedance. Radiation from one driven element induces currents on neighboring elements, which causes the embedded element pattern to differ from the isolated element pattern [10]. The driven element also induces a nonzero voltage at the terminals of other elements [11]. In millimeter microstrip antennas, the size of the antenna is very small. At a distance of λ/2 between two antennas, mutual coupling is crucial due to the propagation of surface waves. Also, it is observed that both increasing the substrate thickness and the permittivity will increase the mutual coupling and the bandwidth is slightly increased [12]. Therefore in the case of high permittivity, it is essential to minimize mutual coupling using new techniques.

This paper presents the design of a single-fed CP antenna for X-band radars, SAR sensors and remote sensing applications. The design is a two-element linear array in the metamaterial substrate. However it is possible to increase the number of elements for an array. The bandwidth requirement must be compatible with a low axial ratio (AR) less than 3 dB to ensure transmitting and receiving CP waves. In order to minimize the mutual coupling between two antenna elements, we describe a simple technique using embedded hexagonal-shaped metamaterial layers between antenna elements. This technique utilizes the hexagonal-split-ring resonators (SRRs) to reduce the mutual coupling between two neighboring patches and does not require an intricate fabrication process. Metamaterials provide effective isolation between microwave circuit elements in specific frequency bands. The basic function of metamaterial insulators is blocking of electromagnetic energy from being transmitted across the insulation boundary. In other words, the hexagonal-SRRs are capable of reducing the surface waves within a certain frequency band. Also, the use

[1]Department of Electrical Engineering, Science and Research Branch, Islamic Azad University, Tehran, Iran
[2]Center of Excellence on Applied Electromagnetic Systems, School of ECE, College of Engineering, University of Tehran, P.O. Box 14395-515, Iran
[3]Faculty of Electrical and Computer Engineering, K. N. Toosi University of Technology, Tehran, Iran
Corresponding author:
M. Naser-Moghadasi
E-mail: mn.moghaddasi@srbiau.ac.ir

of circular rings with parallel line strips provides a more robust CP antenna due to improved phase stability of the feed arrangement.

II. SINGLE-FED CP ANTENNA

A conventional microstrip patch antenna is usually made on a substrate and backed by a conducting ground plane. In the present structure, double back to back SRRs are placed horizontally between the patch and ground plane. In order to maintain the transmission consistency of the input energy, the metal in and around the feed-line area is etched.

A) Metamaterial basic theory

Left-handed metamaterials have received considerable interest due to their unique physical properties. Usually, ε and μ are both positive in ordinary materials. For certain artificial structures, however, both the effective permittivity, ε_{eff} and effective permeability, μ_{eff}, can have negative values. In such media, the electric, magnetic, and wave vector components form a left-handed (LH) coordinate system, hence the name LH material is used for their description. The capacitive elements of SRRs are applied to the resonant behavior, which in turn results in rather high positive and negative values of permeability near the magnetic resonant frequency. The resonance characteristics of SRRs are studied in the literature in order to understand the mechanism behind negative permeability [13]. We first performed simulations to compare with the experimental results. Simulations were performed by using the commercial software high frequency structure simulator (HFSS), which is a three-dimensional (3D) full-wave solver and employs the finite element method. We also measured the transmission coefficient S_{21} of the SRR unit cell using two monopole antennas which were used for transmission and detection of electromagnetic waves through the single SRR unit [14, 15]. The simulated and measured frequency responses of embedded single and double SRRs structures are shown in Fig. 1. A transmission dip is observed at 11.1 GHz throughout the transmission spectrum of a single SRR and a broadband transmission dip at 11 GHz for double SRR structure. Simulations are in good agreement with the experiments.

We also propose a new broadband metamaterial structure composed of a unit cell with multiple hexagonal-shaped metal rings printed one inside the other. The introduced metamaterial structure exhibits multi-resonant behavior due to distinct magnetic resonances caused by the self and mutual coupling of each inclusion. The number of distinct magnetic resonances is determined by the numbers of hexagonal-shaped rings placed in the unit cell. With a magnetic field applied along the z-axis (Fig. 2), an electromotive force appears around the hexagonal-SRR which makes the structure behaves like a L–C network with a resonant frequency, f_o, expressed as:

$$f_o = \frac{1}{2\pi\sqrt{2a_{eq}L_{net}C_{net}}} \tag{1}$$

where a_{eq} is the effective radius, L_{net} is the net inductance and C_{net} is the net effective capacitance of the equivalent L–C network of the hexagonal-SRR [16]. The effective radius, a_{eq}, can be obtained analytically [16], which is given in Appendix A. Using two rings and a hexagonal-plate on the center, three distinct resonant frequencies can be shifted to desired values simply by changing the design parameters which is described in the paper. Transmission and reflection spectra of the proposed structure are obtained and the resonant frequencies are observed.

The simulated and measured frequency responses of an embedded hexagonal-shaped metamaterial layer are shown in Fig. 2. We use this property to reduce the mutual coupling between two antenna elements.

The elements of the S matrix can be obtained from the elements of the T-matrix [17] using the analytic expression for the T-matrix elements:

$$S_{21} = S_{12} = \frac{1}{\cos(nkd) - [i/2](Z(\omega) + 1/Z(\omega))\sin(nkd)}, \tag{2}$$

$$S_{11} = S_{22} = \frac{i}{2}\left(\frac{1}{Z(\omega)} - Z(\omega)\right)\sin(nkd). \tag{3}$$

Here, S_{11} and S_{21} are the reflection and transmission coefficients of the S-parameters, respectively. The wave number k

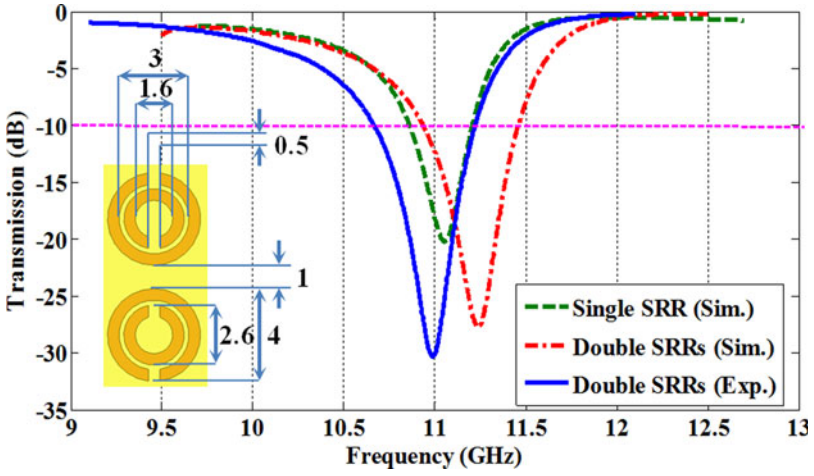

Fig. 1. The frequency responses of an embedded single and double SRR structure.

https://doi.org/10.1017/S1759078715000847 Published online by Cambridge University Press

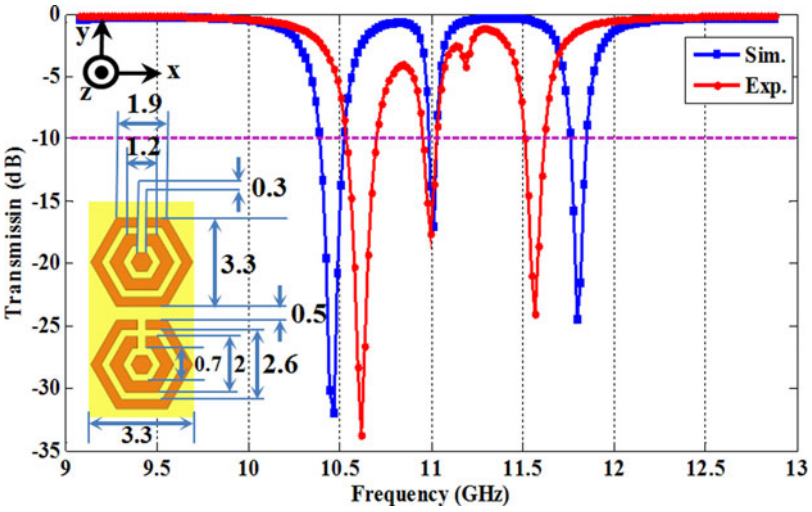

Fig. 2. Frequency responses of an embedded hexagonal-SRR structure. All dimensions are in mm.

is the incident wave number [18]. The incident wave is assumed to travel rightward along the positive x-axis, with the origin defined as the first face of the material seen by the radiation. When characterizing the SRR system to be used as an equivalent homogeneous slab, d is the thickness of such a slab. Equations (2) and (3) can be inverted yielding $Z(\omega)$ and $n(\omega)$ in terms of the scattering parameters:

$$Z(\omega) = \sqrt{\frac{(1+S_{11})^2 - S_{21}^2}{(1-S_{11})^2 - S_{21}^2}}, \tag{4}$$

$$n(\omega) = \frac{1}{kd}\cos^{-1}\left[\frac{1}{2S_{21}}(1 - S_{11}^2 + S_{21}^2)\right] \tag{5}$$

Also, the refractive index and normalized intrinsic impedance of the material can be expressed in terms of $\varepsilon(\omega)$ and $\mu(\omega)$ as:

$$n(\omega) = \sqrt{\mu(\omega) \times \varepsilon(\omega)}, \tag{6}$$

$$Z(\omega) = \sqrt{\mu(\omega)/\varepsilon(\omega)}. \tag{7}$$

In Fig. 3 it can be observed that the real parts of $\varepsilon_r(\omega)$ and $\mu_r(\omega)$ of the proposed structure are matched at 10–11.7 GHz.

B) Antenna design procedure

A radiating semi-circular patch is placed above a dielectric substrate backed by a ground plane. A microstrip single-fed line is used to excite the patch. Two conducting SRRs are placed horizontally between the patch and the ground plane. The geometry of SRRs, shown in Fig. 4(c), is optimized by varying the number of split rings, radius of the largest ring, slot width, metallization width, and gap width. To reduce optimization costs, the values of metallization width and the gap width are chosen to be the same for all of complementary split rings [14].

Figure 4 illustrates the proposed geometry and prototype of a miniaturized circular patch antenna and its dimensions.

We have also optimized the separation of the two rings slightly to achieve a better performance of the antenna. In this connection, the radiation along the patch direction is significantly enhanced.

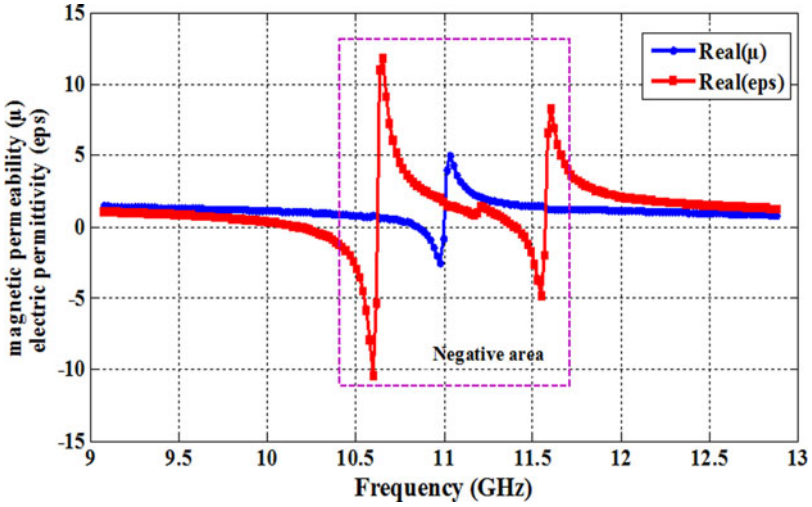

Fig. 3. Results for the two-ring hexagonal-SRR, real parts of the permeability and permittivity.

https://doi.org/10.1017/S1759078715000847 Published online by Cambridge University Press

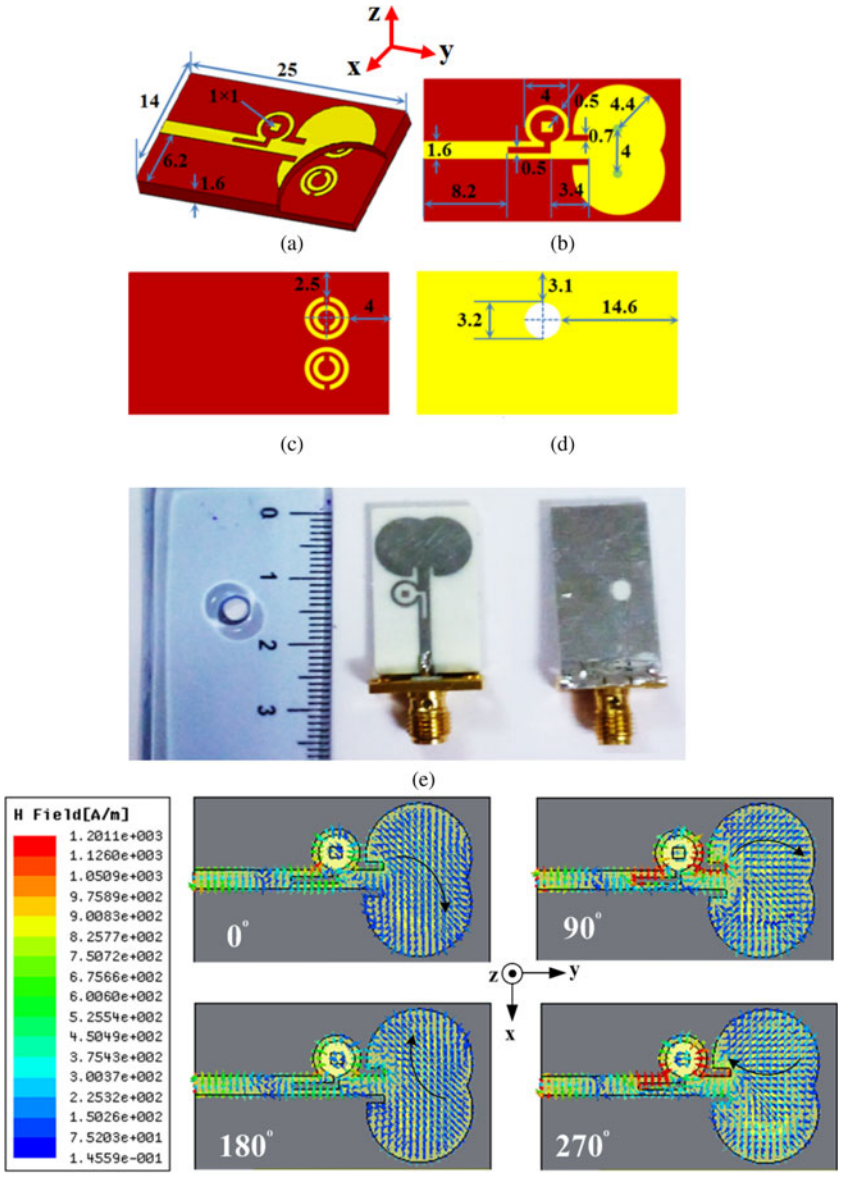

Fig. 4. Geometry and prototype of a miniaturized circular patch antenna and its dimensions; (a) 3D view, (b) antenna element, (c) SRRs structure, (d) ground plane, (e) top and bottom of single element antenna prototype, (f) simulated vector magnetic field distributions at 10.8 GHz. All dimensions are in mm.

C) Feed line for circular polarization

The patch antenna is excited through a microstrip single-line. The antenna is matched through a quarter-wavelength microstrip line transformer with stubs and their dimensions optimized to enhance the matching between the antenna and the 50Ω microstrip line. The excitation line has a delay ring to provide the circular polarization. The method of analysis used here follows the conventional approach adopted for coupled microstrip lines. In addition, the coupling is carefully controlled by microstrip circular ring resonator and the tuning is performed by changing the radius of the ring. By using the correct amount of delay, the signal can be shifted for the intended amount of phase shift [19, 20]. A circular-shape slot is cut in the ground plane as shown in Fig. 4(d) and its dimensions are optimized to enhance the circular polarization. It can be seen that a high level of electromagnetic coupling is present between the delay ring and the upper end of the radiant patch. This effect together with that due to the circular slots etched on the ground plane is responsible for the excitation of the circular polarization. In fact, the circular ring appears to behave more like a device breaking the symmetry of the structure, and coupling strongly with the upper edge of the radiating patch. This coupling is able to excite a circular polarization. Figure 4(f) shows the magnetic field distributions excited on the feeding line and the radiating element for four different instants (phase of magnetic field) i.e. $\omega t = 0^\circ$, 90°, 180°, and 270°. It is noted that the vector magnetic field distributions at $\omega t = 180^\circ$ and 270° are equal in magnitude and opposite in phase of $\omega t = 0^\circ$, 90°, respectively. Therefore, it can be concluded that the magnetic field vector rotates in the right-hand direction by 90° in $+z$-direction after a quarter-period, which satisfies the requirement of the spatial and temporal quadrature for circular polarization. As for $-z$-direction, the direction in

https://doi.org/10.1017/S1759078715000847 Published online by Cambridge University Press

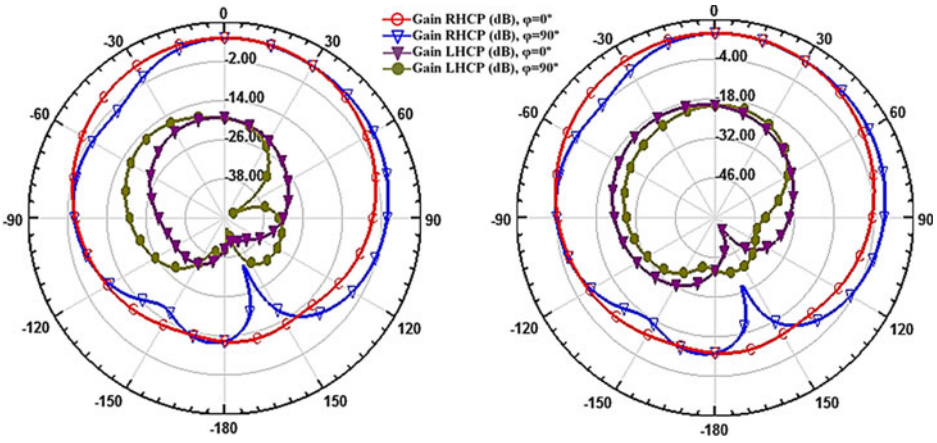

Fig. 5. The proposed antenna, (a) simulated and (b) measured polar radiation pattern, at 10.8 GHz in the *xz*-plane ($\varphi = 0^\circ$) and the *yz*-plane ($\varphi = 90^\circ$).

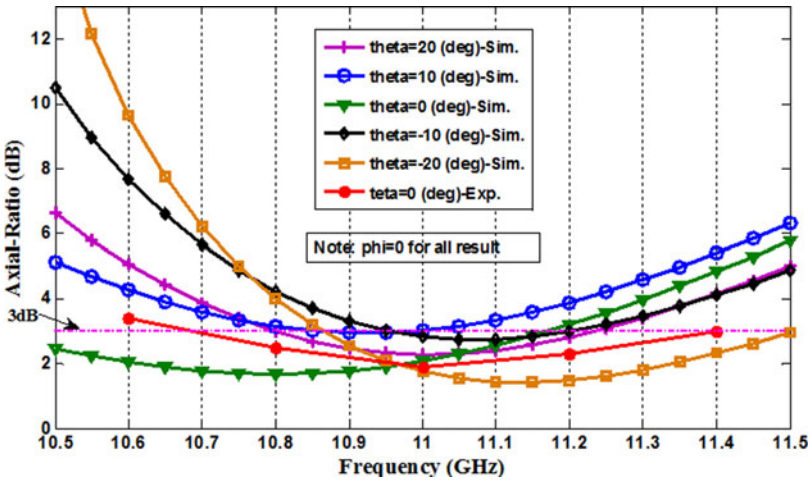

Fig. 6. Simulated and measured antenna AR at different deviations from the center frequency.

which the magnetic field vector rotates is opposite to that of $+z$-direction, i.e. the proposed CP antenna generates right hand circular polarization (RHCP) in $+z$-direction while left hand circular polarization (LHCP) in $-z$-direction [21]. In addition, since the levels of the surface current density along the edge of the radiator are higher, the emission of electromagnetic energy mainly takes place from the regions located along the edges of the radiating patch [21].

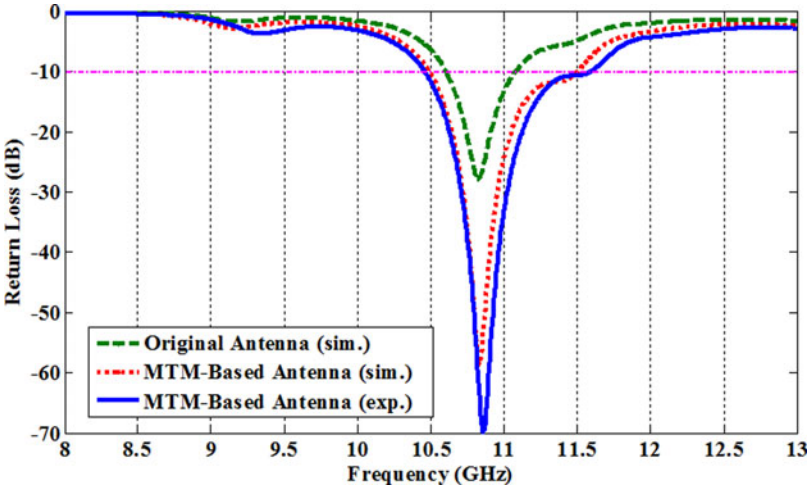

Fig. 7. Simulated and measured return loss for single antenna.

https://doi.org/10.1017/S1759078715000847 Published online by Cambridge University Press

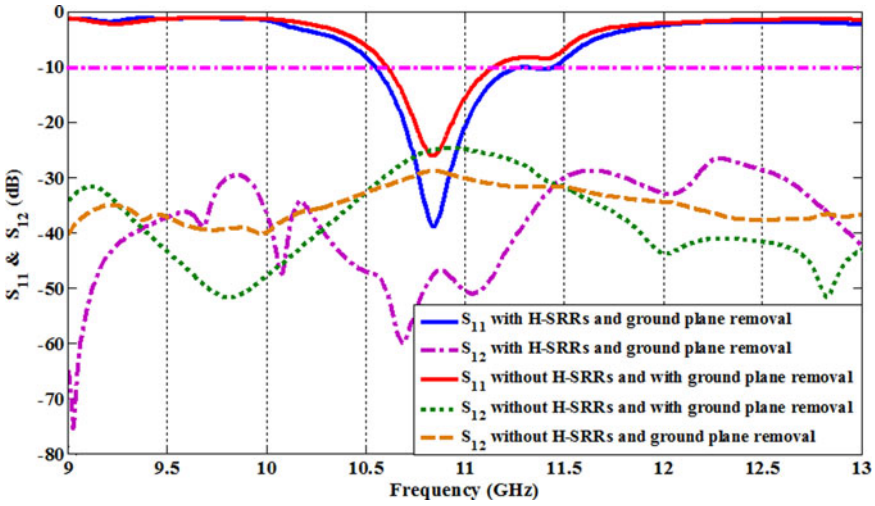

Fig. 8. Simulated *S*-parameters for array antenna in the different structures.

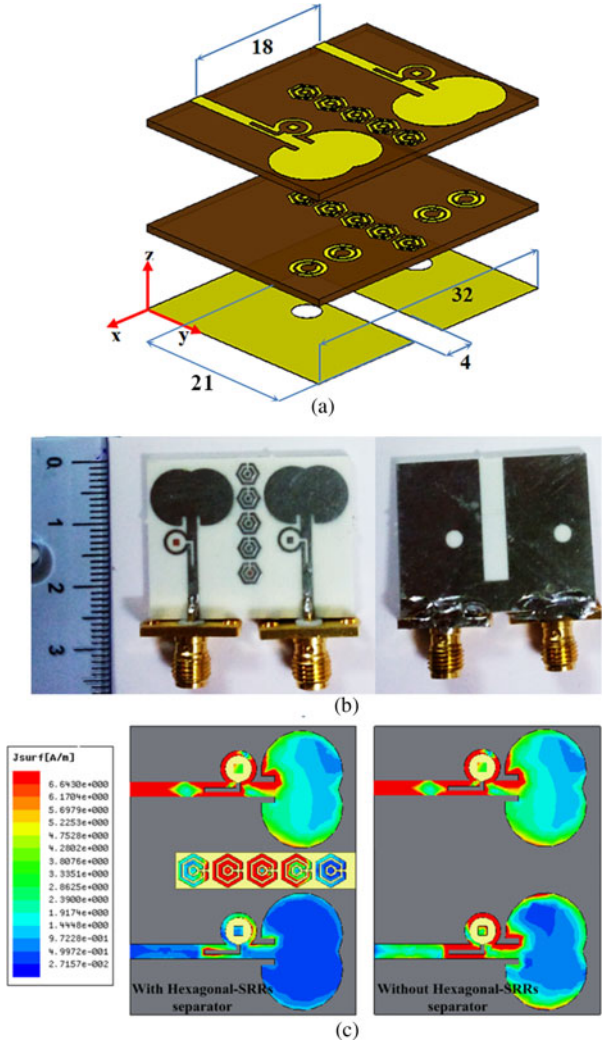

Fig. 9. Geometry and prototype of array antenna and its dimensions in mm; (a) 3D view, (b) top and bottom view of the antenna. (c) Simulated surface currents intensity at the resonant frequency.

Figure 5 presents the proposed antenna radiation pattern from which, the antenna introduces RHCP performance. The proposed antenna has 3 dB AR bandwidth of 800 MHz as shown in Fig. 6 which covers the required band.

The proposed patch antenna was designed, simulated, fabricated, measured, and comparatively studied with theoretical results. The prototype CP antenna was fabricated on Rogers RO4003 dielectric substrate, which has a thickness of 1.6 mm, a relative permittivity of 3.38, and loss tangent of 0.003. The substrate was plated with 1 oz Copper. To optimize the design for various parameters, a full wave finite element method simulator was used. The simulated and measured S_{11} values of the proposed antenna and the patch antenna without SRRs are obtained and shown in Fig. 7. As is observed, the operating bandwidth of the conventional patch antenna is 400 MHz (around 10.5 GHz), which is typically wide. The proposed antenna is designed to have 1 mm gap between SRRs, and the −10 dB bandwidth within 10.4–11.6 GHz range. The bandwidth is 1.2 GHz and is three times wider than the bandwidth of the conventional antenna.

III. MUTUAL COUPLING REDUCTION

When two CP antenna elements are brought in the vicinity of each other, the current in each element changes in both amplitude and phase. We introduce the coupling path term in order to account for the mutual coupling between antennas and the current path through the displacement current. A hexagonal-SRR metamaterial is developed in order to efficiently suppress the electromagnetic coupling between closely-spaced antenna elements. The hexagonal-SRRs considered here have equal sides with strip widths of 0.5 mm. The rings with small gaps are etched on and in the dielectric substrate in two rows. The cut gaps within the metallic rings are 0.5 mm. The total size of the dielectric substrate is 30 × 25 mm^2 with a thickness of 1.6 mm. The hexagonal-SRRs are made of copper with a thickness of 20 μm.

By embedding the hexagonal-SRRs array between the antenna elements, as shown in Fig. 8, the mutual coupling has been reduced by about 26.6 dB at the resonant frequency,

https://doi.org/10.1017/S1759078715000847 Published online by Cambridge University Press

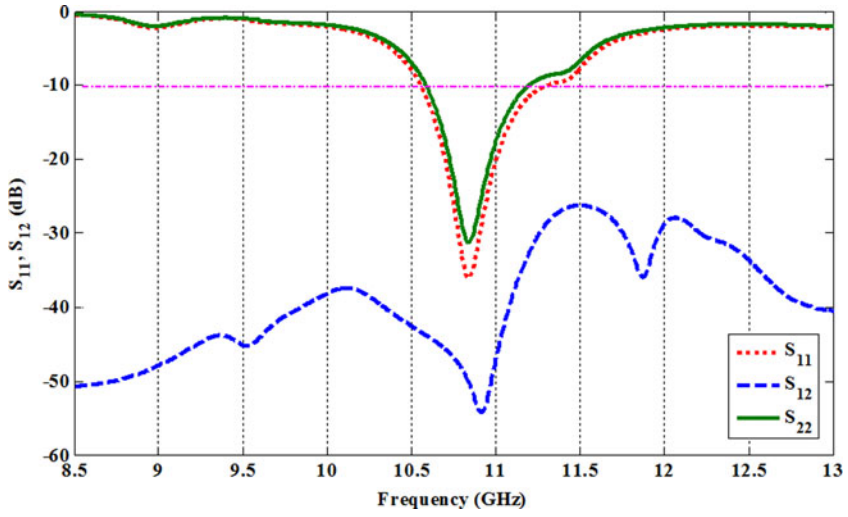

Fig. 10. Measured *S*-parameters for the array antenna.

while maintaining good impedance match for the two-antenna system. The simulation results are presented in the different structures with and without hexagonal-SRRs and their associated ground plane.

IV. ANTENNA FABRICATION AND MEASUREMENT RESULTS

A) Array antenna fabrication

The sandwich structure consists of two thin load-bearing face sheets. Each layer must meet its own combination of structural and electrical design requirements, as well as the manufacturing and assembly requirements. The basic panel layers are: antenna elements, metamaterial structure, and the defected ground layer. It is worth mentioning that human errors caused by manual cutting and soldering of shorted annular rings can deform the antenna elements, thereby shifting the resonant frequency as well as degrading the polarization purity. Figure 9(a) shows the layered structure and front and back of the manufactured antenna prototype. In addition, the photograph of the manufactured antenna is shown in Fig. 9(b). Figure 9(c) shows the calculated current distribution on the CP antenna array at 10.8 GHz and shows that the surface current of the active antenna has little impact on the adjacent antenna.

B) Array measurement results

The measured *S*-parameters of the proposed antenna array with hexagonal-SRRs are obtained and shown in Fig. 10. Far-field radiation patterns for the CP antennas with- and without-SRRs are numerically computed using HFSS in order to quantify the performance of the antenna system. The antenna's radiation pattern measurements were performed in an anechoic chamber. A wideband (2–18 GHz) standard CP horn antenna was used as field probe and the antenna gain and radiation patterns were measured for RHCP and LHCP field components.

The measured far field radiation patterns of this antenna for active element are shown in Fig. 11 at 10.8 GHz for LHCP and RHCP components. We used a standard linear polarization horn in the case of the linear polarization measurement for co-polarized and cross-polarized field components.

Figure 12 compares the co-polarized with cross-polarized patterns of the array antenna at 10.8 GHz and shows the measured cross-polarization levels are approximately equal with the co-polarization levels which are a good result for CP antenna. The corresponding gains of *E*-left and *E*-right are -21.3 and -5.8 dBi, respectively, at $\varphi = 0^\circ$. This agrees well with the finding obtained from the simulated radiation patterns by HFSS. Also, Table 1 gives the comparison of the final antenna with and without hexagonal-SRRs.

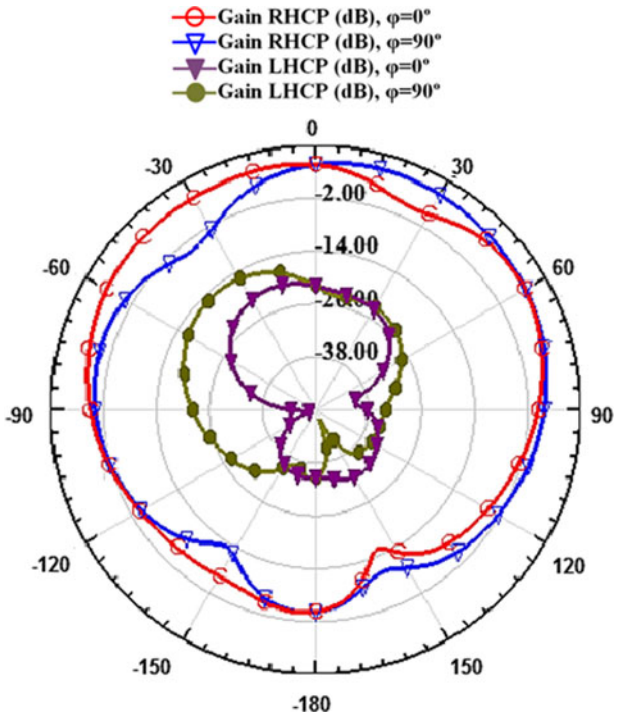

Fig. 11. Measured polar radiation patterns for array antenna for active element at 10.8 GHz in the *xz*-plane ($\varphi = 0^\circ$) and the *yz*-plane ($\varphi = 90^\circ$).

https://doi.org/10.1017/S1759078715000847 Published online by Cambridge University Press

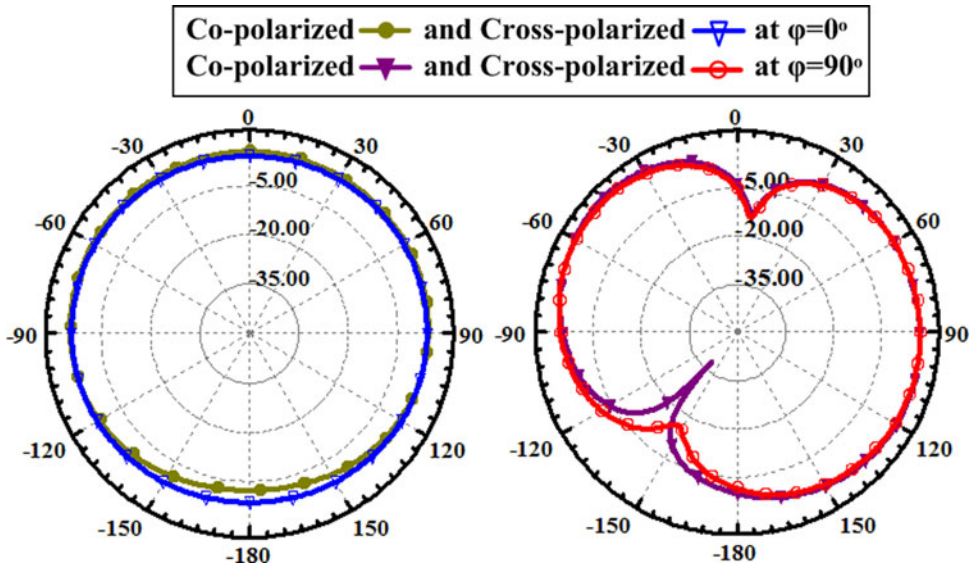

Fig. 12. Measured radiation patterns of co-polarization and cross-polarization for the active element at 10.8 GHz in the *xz*-plane ($\varphi = 0^\circ$) and the *yz*-plane ($\varphi = 90^\circ$).

Table 1. Comparison between the antenna arrays with and without hexagonal-SRRs.

Performance parameter	Without hexagonal-SRRs	With hexagonal-SRRs
Frequency	10.8 GHz	10.8 GHz
Bandwidth	1.0 GHz	1.2 GHz
S_{11}, S_{12}	−27, −25 dB	−38, −51.6 dB
Gain	6.1 dBi	6.2 dBi
Axial ratio	2.0 dB	2.1 dB

We have used a reverberation chamber with dimension $3.2 \times 2.2 \times 3$ m^3 for antenna gain and efficiency measurement using the method described in references [22, 23]. The measured power of the antenna at 10.8 GHz for the single and the array structure were approximately −38.2 and −38.1 dBm, respectively. In comparison standard antenna provides about −36.1 dBm of power. The standard antenna is better by 2.1 and 2 dBs than a single CP-antenna and the array structure, respectively. Thus, the efficiency for the proposed antenna and the array in 10.8 GHz is 61.6 and 63%, respectively.

V. CONCLUSION

In this paper, mutual coupling between closely-spaced printed CP antennas is investigated particularly for radars and GNSS remote sensing, specifically at X band. Two-element microstrip arrays with back-to-back embedded SRRs are studied and by suppressing the surface waves using hexagonal-SRRs, it provides a very low mutual coupling between array elements. The studies indicate that, compared with the conventional array, the mutual coupling in the array loaded by mu-negative (MNG) is suppressed effectively, and the new array has a better performance. A reduction in mutual coupling of 21 dB at 10.8 GHz was achieved for the antenna system with MNG while the −10 dB bandwidth maintained the same.

ACKNOWLEDGEMENT

The authors would like to thank the Faculty of Eng., Science & Research Branch, Islamic Azad University, Tehran, for their support in performing the antenna measurements.

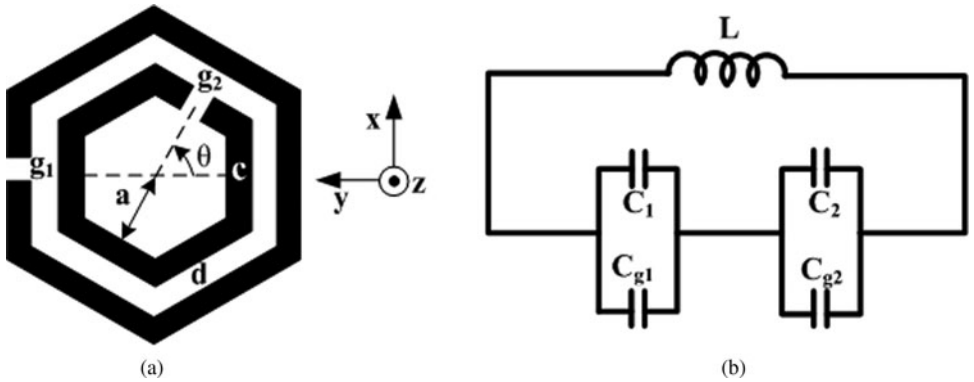

Fig. 13. Schematic geometry of (a) a hexagonal-SRR and (b) its equivalent circuit model.

https://doi.org/10.1017/S1759078715000847 Published online by Cambridge University Press

REFERENCES

[1] Li, Y.; Li, W.; Yu, W.: A switchable UWB slot antenna using SIS-HSIR and SIS-SIR for multi-mode wireless communications applications. ACES J., **27** (4) (2012), 340–351.

[2] Lin, Y.; Kao, Y.; Pan, S.; Chen, H.: Bidirectional radiated circularly polarized annular-ring slot antenna for portable RFID reader. ACES J., **25** (3) (2010), 182–189.

[3] Rezaeieh, S.A.; Şimşek, S.; Pourahmadazar, J.: Design of a compact broadband circularly-polarized slot antenna for wireless applications. Microw. Opt. Technol. Lett., **55** (2) (2013), 413–418.

[4] Rahim, S.A.; Danesh, Sh.; Okonkwo, U.A.; Sabran, M.; Khalily, M.: UWB monopole antenna with circular polarization. Microw. Opt. Technol. Lett., **54** (4) (2012), 949–953.

[5] Ma, J.; Kouki, A.B.; Landry, R. Jr.: "Wideband circularly polarized single probe-fed patch antenna. Microw. Opt. Technol. Lett., **54** (8) (2012), 1803–1808.

[6] Shanmugam, B.; Sharma, S.K.: Investigations on a novel without Balun modified Archimedean spiral antenna with circularly polarized radiation patterns. ACES J., **27** (8) (2013), 676–684.

[7] Maqsood, M.; Bhandari, B.; Gao, S.; Steenwijk, R.D.; Unwin, M.: Development of dual-band circularly polarized antennas for GNSS remote sensing onboard small satellites, Presented at the ESA Workshop on Antennas for Space Applications, ESTEC, The Netherlands, 2010.

[8] Imbraile, W.; Gao, S.; Boccia, L.: Space Antenna Handbook, Wiley, Hoboken, NJ, 2012.

[9] Jiang, Y.; Yang, H.; Wang, X.: The design and simulation of an S-band circularly polarized microstrip antenna array, Presented at the Symp. Progress in Electromagnetics Research, Xi'an, China, March 22–26, 2010.

[10] Bait-Suwailam, M.M.; Siddiqui, O.F.; Ramahi, O.M.: Mutual coupling reduction between microstrip patch antennas using slotted-complementary split-ring resonators. IEEE Antennas Wireless Propag. Lett., **9** (2010), 876–878.

[11] Simon, R.; Zavala, A.: Antenna and Propagation for Wireless Communication Systems, 2nd ed., John Wiley & Sons Ltd, Chichester, 2007.

[12] Farahbakhsh, A.; Moradi, G.; Mohanna, S.: Reduction of mutual coupling in microstrip array antenna using polygonal defected ground structure. ACES J. Paper, **26** (4) (2011), 334–339.

[13] Bilotti, F.; Alu, A.; Vegni, L.: Design of miniaturized metamaterial patch antennas with μ-negative loading. IEEE Antennas Wireless Propag. Lett., **56** (6) (2008), 1640–1647.

[14] Aydin, K.; Bulu, I.; Guven, K.; Soukoulis, M.K.C.M.; Ozbay, E.: Investigation of magnetic resonances for different split-ring resonator parameters and designs. IOP Sci. New J. Phys., **7** (2005), 168.

[15] Rhode & Schwarz: Measurement of Dielectric Material Properties. RAC-0607 0019_1_5E, Application Notes, April 2012.

[16] Marquez, R.; Mesa, F.; Martel, J.; Medina, F.: Comparative analysis of edge- and broadside-coupled split ring resonators for metamaterial design-theory and experiments. IEEE Trans. Antennas Propag., **51** (2003), 2572–2581.

[17] Smith, D.R. et al.: Electromagnetic parameter retrieval from inhomogeneous metamaterial. Phys. Rev. E, **71** (2005), 036617.

[18] Smith, D.R.; Schultz, S.; Markos, P.; Soukoulis, C.M.: Determination of effective permittivity and permeability of metamaterials from reflection and transmission coefficients. Phys. Rev. B, **65** (2002), 195104.

[19] Villegas, J.M.; Andrade, A.; Dueñas, A.: Testing the applicability of a hybrid FDTD-MoL technique on the simulation of passive microstrip paths. Int. J. Microw. Opt. Technol., **4** (6) (2009), 344–348.

[20] Mongia, R.K.; Bahl, I.J.; Bhartia, P.; Hong, J.: RF and Microwave Coupled-Line Circuits, 2nd ed. Artech House, Norwood, MA, 2007.

[21] Caratelli, D.; Cicchetti, R.; Bit-Babik, G.; Faraone, A.: Circuit model and near-field behavior of a novel patch antenna for WWLAN applications. Microw. Opt. Technol. Lett., **49** (1) (2007), 97–100.

[22] Khaleghi, A.; Bolomey, J.C.; Azoulay, A.: On the statistics of reverberation chambers and applications for wireless antenna test, in Proc. IEEE Int. Symp. on Antennas and Propagation (AP-S), Albuquerque, NM, July 2006, 3561–3564.

[23] Kalliola, K.; Sulonen, K.; Laitinen, H.; Kivekas, O.; Krogerus, J.; Vainikainen, P.: Angular power distribution and mean effective gain of mobile antenna in different propagation environments. IEEE Trans. Veh. Technol., **51** (5) (2002), 823–838.

[24] Bashenoff, V.J.: Abbreviated methods for calculating the inductance of irregular plane polygons of round wire, in Proc. of Institute of Radio Engineers, 1927.

[25] Terman, F.E.: Radio Engineers Handbook, McGraw-Hill, New York, 1943.

[26] Bose, S.; Ramaraja, M.; Dr. Raghavana, S., Kumara, S.: Mathematical modeling, equivalent circuit analysis and genetic algorithm optimization of an N-sided Regular Polygon Split ring Resonator (NRPSRR). 2nd Int. Conf. Commun. Comput. Secur. Procedia Technol., **6** (2012), 763–770.

APPENDIX

Applying general trigonometry to Fig. 13, and assuming $g_1 = g_2 = g$, we estimate the effective radius, a_{eq}, as [16]:

$$a_{eq} = a - \frac{g}{6}. \tag{A.1}$$

L can be analytically expressed as:

$$L = \frac{\mu_0 \pi^2}{I^2} \int_0^\infty [\mathfrak{T}(k)]^2 k^2 \, dk, \tag{A.2}$$

where $\mathfrak{T}(k)$ is the Fourier-Bessel transform of the current, I, excited on the metal ring [16]. For computational convenience, Bashenoff deduced a simpler expression to compute the self-inductance of any closed loop conductor using semi-empirical methods [24]. Simplified further by Terman [25], the net inductance, L_{net} can be analytically expressed as:

$$L_{net} = 0.00508 \cdot l \left(2.303 Ln \frac{4l}{\rho} - 2.636 \right), \tag{A.3}$$

where l the perimeter of the Hexagonal-SRR (equal to $6a$) and ρ is the width of the cross-section of the conductor (equal to c); and μ is the permeability of the conductor. Considering the rotation of inner ring by angle θ in counter-clockwise direction as shown in Fig. 13, we express θ as:

$$\theta = m\frac{\pi}{3} + \psi, \tag{A.4}$$

where m is some integer and $\psi < 2\pi/6$. For this counter-clockwise rotation of angle θ, the perimeter of the upper half-ring decreases and that of lower half-ring increases by

https://doi.org/10.1017/S1759078715000847 Published online by Cambridge University Press

an amount Δ, computed using general trigonometry as:

$$\Delta = \frac{a}{2}\left\{(2m+1) - \sqrt{3}\tan\left(\frac{\pi}{6} - \psi\right)\right\}. \quad (A.5)$$

Now the capacitance of the upper half-ring, C_u, and lower half-ring, C_l can be easily computed from Δ & C_{pul} as [26]:

$$C_u = \left(\frac{a}{3} - \Delta\right)\cdot C_{pul}, \quad C_l = \left(\frac{a}{3} + \Delta\right)\cdot C_{pul}, \quad (A.6, 7)$$

where C_{pul} is estimated as [26]:

$$C_{pul} = \varepsilon_0 \cdot \left(\frac{\varepsilon_r + 1}{2}\right)\frac{\sqrt{1-\sigma^2}}{\mathcal{E}(\sigma)}, \quad (A.8)$$

with $\sigma = d/(d+2c)$ and $\mathcal{E}(\cdot)$ is the complete elliptical integral of the second kind, defined as:

$$\mathcal{E}(\sigma) = \int_0^{\pi/2} \sqrt{1-(\sigma\sin\theta)^2}\, d\theta. \quad (A.9)$$

The capacitance due to the gaps (splits) in the hexagonal-SRR, C_g can be estimated using parallel plate approximation method, while assuming $g_1 = g_2 = g$, as:

$$C_g = \frac{\varepsilon_0 \cdot \varepsilon_r \cdot c \cdot h}{g}, \quad (A.10)$$

where h is the depth of substrate on which SRR is embedded. Note that equation (A.10), providing a very approximate expression of the exact value of the capacitance C_g, can be used just to get an idea of how the resonant ring behaves.Therefore, the net equivalent capacitance of the L–C network, C_{net}, stands out to be:

$$\frac{1}{C_{net}} = \frac{1}{(C_u + C_g)} + \frac{1}{(C_g + C_l)}, \quad (A.11)$$

which can be simplified using general algebra and expressed as:

$$C_{net} = \frac{(C_u + C_g)(C_g + C_l)}{(C_u + 2C_g + C_l)}. \quad (A.12)$$

Thus by using equations (A.1), (A.3), and (A.12) in equation (1) and the equivalent circuit shown in Fig. (13), we can determine the resonant frequency of the hexagonal-SRR. Solving $\partial f_0/\partial\theta = 0$ for minimization of f_0, gives us minimum f_0 at $\theta = 180^\circ$.

R. Hafezifard received the M.Sc. and Ph.D. degrees in wave communication from Department of Electrical Engineering, Science and Research Branch, Islamic Azad University, Tehran, Iran, Iran in 2010 and 2015, respectively. He recently worked in aerospace organization of Iran, on waveguides and antennas design, simulation and manufacturing and radar systems. From 2010, he was a Research Assistant with the department of engineering, Islamshar branch, IAU, Iran. His research interest includes the development of electromagnetic proprieties of metamaterial and PEMC.

Jalil Rashed–Mohassel received the M.Sc. degree in electronics engineering from University of Tehran, Tehran, Iran in 1976 and the Ph.D. degree in electrical engineering from the University of Michigan, Ann Arbor, in 1982. Formerly he was with the university of Sistan and Baluchestan, Zahedan, Iran, where he held several academic and administrative positions. In 1994 he joined University of Tehran, Tehran, Iran, where he is teaching and performing research as a Professor in antennas, EM theory and applied mathematics. He served as the academic Vice-Dean in College of Engineering and Vice-Chairman, School of Electrical and Computer Engineering. Currently, he is the General Director for academic affairs of the university, a member of Center of Excellence in Applied Electromagnetic Systems and the Director of the microwave laboratory.

Mohammad Naser-Moghadasi was born in Saveh, Iran, in 1959. He received the B.Sc. degree in Communication Eng. in 1985 from the Leeds Metropolitan University (formerly Leeds polytechnic), UK. Between 1985 and 1987 he worked as an RF design engineer for the Gigatech company in Newcastle Upon Tyne, UK. From 1987 to 1989, he was awarded a full scholarship by the Leeds educational authority to pursue an M.Phil. Studying in CAD of Microwave circuits. He received his Ph.D. in 1993, from the University of Bradford, UK. He was offered then a two years Post Doc. To pursue research on Microwave cooking of materials at the University of Nottingham, UK. From 1995, Dr. Naser-Moghadasi joined Islamic Azad University, Science and Research Branch, Iran-Tehran, where he currently is head of postgraduate studies. His main areas of interest in research are Microstrip antenna, Microwave passive and active circuits, RF MEMS. Dr. Naser-Moghadasi is member of the Institution of Engineering and Technology, MIET and the Institute of Electronics, Information and Communication Engineers (IEICE). He has so far published over 150 papers in different journals and conferences.

Ramezan Ali Sadeghzadeh received his B.Sc. in 1984 in telecommunication Engineering from the Khajeh Nassir Toosi, University of Technology, Tehran, Iran, and M.Sc. in digital Communications Engineering from the University of Bradford and UMIST (University of Manchester, Institute of Science and Technology), UK, as a joint program in 1987. He received his Ph.D. in electromagnetic and antenna from the University of Bradford, UK, in 1990. He worked as a Post- Doctoral Research assistant

https://doi.org/10.1017/S1759078715000847 Published online by Cambridge University Press

in the field of propagation, electromagnetic, antenna, Bio-Medical, and Wireless communications from 1990 till 1997. From 1984 to 1985 he was with Telecommunication Company of Iran (TCI) working on Networking. Since 1997 he is with K.N.Toosi University of Technology working with Telecommunications Dept. at faculty of Electrical and Computer Engineering. He has published more than 75 referable papers in international journals and conferences. Dr. Sadeghzadeh's current interests are numerical techniques in electromagnetic, antenna, propagation, radio networks, wireless communications, nano-antennas, and radar systems.

https://doi.org/10.1017/S1759078715000847 Published online by Cambridge University Press